# Heat transfer measurements in rotating-disc systems
# Part 2: The rotating cavity with a radial outflow of cooling air

**A. Northrop and J. M. Owen**
Thermo-Fluid Mechanics Research Centre, School of Engineering & Applied Sciences, University of Sussex, Sussex, UK

*Received 28 February 1987; accepted 11 June 1987*

A comparison between theoretical and experimental results is presented for the flow and heat transfer in a rotating cavity with a radial outflow of cooling air for a range of rotational Reynolds numbers up to $Re_\phi = 3.3 \times 10^6$ and dimensionless flow rates up to $C_w = 14{,}000$. Flow visualization confirmed that the flow structure comprises a source region, Ekman layers, a sink layer, and an interior core of rotating fluid, and measured values of the size of the source region are in good agreement with a simple theoretical model. Except at high flow rates and low rotational speeds, where the source region fills the entire cavity, the agreement between the measured and theoretically determined local Nusselt numbers is mainly good. A maximum value of Nusselt number occurs at the approximate edge of the source region, and Nu increases with increasing $C_w$ and $Re_\phi$. The radial distribution of temperature has a significant effect on the Nusselt numbers, particularly in the Ekman-layer region, and under some conditions negative values of Nu have been predicted and measured.

**Keywords:** heat transfer; rotating disc; rotating cavity

## Introduction

A rotating cylindrical cavity, formed by two plane corotating discs and a cylindrical shroud, provides a simple model of the more complex geometry that exists in gas turbine rotors. In the advanced gas turbine, cooling air is extracted from the compressor, and some of this air is used to remove the heat, generated by windage and by conduction down the blades, from the turbine discs. The flow and heat transfer between the corotating turbine discs depends, among other things, on the flow rate of the cooling air and on the rotational speed of the discs, and it is also affected by the radial distribution of temperature in the discs themselves. During takeoff, the turbine blades of an aeroengine heat rapidly, and the outer edge of the disc becomes hotter than the center; during deceleration or landing conditions, the reverse may be true. If the turbine designer is to predict accurately the stress, growth and life of the discs, then knowledge of the heat transfer processes is essential.

Part 1 of this two-part paper (cited in Ref. 1 and referred to below as I) was concerned solely with heat transfer from a single disc rotating in a quiescent environment, the so-called free disc. The Nusselt numbers obtained for a range of rotational Reynolds numbers and for different radial distributions of temperature were found to agree reasonably well with existing theoretical models. In Part 2, the results of flow visualization and heat transfer measurements, conducted inside a rotating cavity with a radial outflow of cooling air, are presented. The relevant literature is reviewed in the second section; the apparatus and data analysis are described in the third section. In the fourth section experimental measurements are compared with theoretical predictions.

## Flow and heat transfer in rotating cavities

Flow and heat transfer in rotating cavities with a radial inflow or outflow of fluid have been studied extensively.[2-9] Figure 1 shows a schematic diagram of the isothermal flow structure for the outflow case in which there is a source region around the inlet, Ekman layers on each disc, a sink layer on the shroud, and an interior core of rotating fluid. With a radial inlet, flow enters uniformly at $r = a$ and is entrained equally into the boundary layers in the source region. With an axial inlet, the incoming flow can impinge on the downstream disc and form a wall jet in the source region.

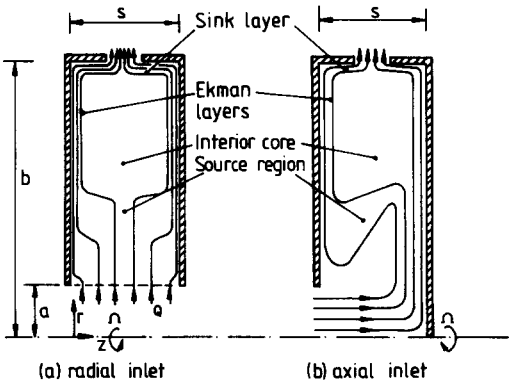


*Figure 1* Schematic diagram of the flow structure inside a rotating cavity with a radial outflow of fluid

At this stage, it is convenient to distinguish Ekman layers from conventional boundary layers. If, for a rotating fluid, the Coriolis forces dominate over inertial forces, Ekman layers form on the rotating discs. Under these conditions, which occur when the relative speed between the disc and the fluid is small, the nonlinear inertial terms in the boundary layer equations (expressed in a frame of reference rotating with the disc) can be ignored, and the resulting "linear Ekman layer equations" can be readily solved.

Owen, Pincombe, and Rogers[6] used momentum integral techniques to solve both the linear and nonlinear equations for isothermal laminar and turbulent flows in a rotating cavity with a radial inflow or outflow of fluid. From the linear theory, the tangential component of velocity in the interior core was found to be identical for laminar and turbulent flows when $Re_r = 180$, and velocity measurements confirmed that this value of $Re_r$ could be used as a criterion for transition from laminar to turbulent flow in the Ekman layers.

In Ref. 6, the size of the source region was estimated for the radial inlet case by assuming that its radius, $r_e$, corresponded to the point at which all the fluid entering the cavity had been entrained into the boundary layers on the two discs. However, if all the fluid impinges on the downstream disc, as may be the case with an axial inlet, the value of $r_e$ is larger than for the radial inlet case. The corresponding solutions for the nondimensional radius of the source region, $x_e$, can be expressed in terms of the nondimensional flow rate, $C_w$, and rotational Reynolds number, $Re_\phi$, by

$$\begin{aligned} x_e &= AC_w^{1/2}Re_\phi^{-1/4} \quad \text{for laminar flow} \\ x_e &= BC_w^{5/13}Re_\phi^{-4/13} \quad \text{for turbulent flow} \end{aligned} \tag{1}$$

where $A = 0.424$ and $B = 1.37$ when the flow is equally distributed between the two discs; $A = 0.599$ and $B = 1.79$ when a wall jet forms. For small values of $x_e$, an axial jet does not always impinge on the downstream disc: the boundary layer suction on the upstream disc can destroy the axial momentum of the incoming jet, and the flow is then distributed equally between the two discs. Regardless of inlet conditions, outside the source region the flow rate in each Ekman layer is, for isothermal flow, invariant with radius and equals half the incoming flow rate.

Northrop and Owen[10] obtained solutions of the turbulent energy integral equation using results derived from the linear Ekman layer equations and ignoring the presence of the source region. For $(T_S - T_I) \propto x^{13/8}$ and a Prandtl number of unity, their solution gives

$$Nu = \frac{13}{32\pi}\frac{C_w}{x}\left\{1 - \exp\left[-0.665C_w^{-5/8}Re_\phi^{1/2}x^{13/8}\right]\right\} \tag{2}$$

where the Nusselt number is defined as

$$Nu = \frac{qr}{k(T_S - T_I)} \tag{3}$$

where $q$ is the heat flux from the disc to the fluid, and $T_S$ and $T_I$ are the respective temperatures of the disc and of the coolant at the cavity inlet. Equation 2 shows similar characteristics to their measured Nusselt numbers, but, except for results obtained at $C_w = 1400$, it tends to overestimate the measurements.

Chew and Rogers[11] extended the momentum integral technique used in Ref. 6 to solve the energy integral equation, including the effects of viscous dissipation, of nonunity Prandtl numbers, and of arbitrary temperature profiles on the discs. For the source region, they assumed that the flow is entrained into the boundary layers from a quiescent fluid. When half the incoming flow has been entrained into each boundary layer, the flow rate is kept constant and the rotational speed of the fluid core adjusts accordingly. In the fourth section a program based on this method is used to compute the local Nusselt numbers, with the measured surface temperatures providing the thermal boundary condition.

## Experimental apparatus, instrumentation, and data analysis

### *The rotating-cavity rig*

For the heat transfer tests, the rotating cavity was formed from two composite discs and a peripheral shroud, as shown in Figure 2, and the whole assembly was designed for rotational speeds up to 5000 r/min. The discs, which had inner and outer diameters of 152 and 950 mm, were spaced an axial distance $s = 59$ mm apart for the heat transfer tests. Each disc was fitted with five internal annular heating elements; further details of their construction, mounting, and instrumentation are given in I.

The shroud used for the heat transfer tests was of composite construction comprising two hiduminium rings ($k = 184$ W/m K) of 5 mm radial thickness and two layers of Rohacell insulation ($k = 0.05$ W/m K). This reduced the effective outer radius $b$ of the cavity to 428 mm and produced a gap ratio of $G = s/b = 0.138$ and a radius ratio of $a/b = 0.104$. Cooling air left the cavity through 32 holes of 9 mm diameter located at equal angular intervals midway between the two discs.

For the flow visualization tests, a transparent polycarbonate shroud of 2 mm thickness was used, and the upstream composite disc was replaced by a polycarbonate disc of 12 mm thickness. For these tests, the hole configuration in the shroud

## Notation

| | |
|---|---|
| $a, b$ | Inner radius and outer radius of cavity |
| $A, B$ | Constants in Equation 1 |
| $C_w = Q/\nu b$ | Nondimensional flow rate |
| $G = s/b$ | Gap ratio |
| $k$ | Thermal conductivity |
| $Nu = qr/k(T_S - T_I)$ | Local Nusselt number |
| Pr | Prandtl number |
| $q$ | Heat flux from disc to cooling air |
| $Q$ | Volumetric flow rate |
| $r$ | Radial coordinate |
| $Re_r = C_w/2\pi x$ | Radial Reynolds number |
| $Re_\phi = \Omega b^2/\nu$ | Rotational Reynolds number |
| $s$ | Axial spacing between discs |
| $T$ | Temperature |
| $x = r/b$ | Nondimensional radial coordinate |
| $z$ | Axial coordinate |
| $\nu$ | Kinematic viscosity |
| $\Omega$ | Angular speed of cavity |
| *Subscripts* | |
| e | Edge of source region |
| I | Inlet condition |
| S | Surface of disc |

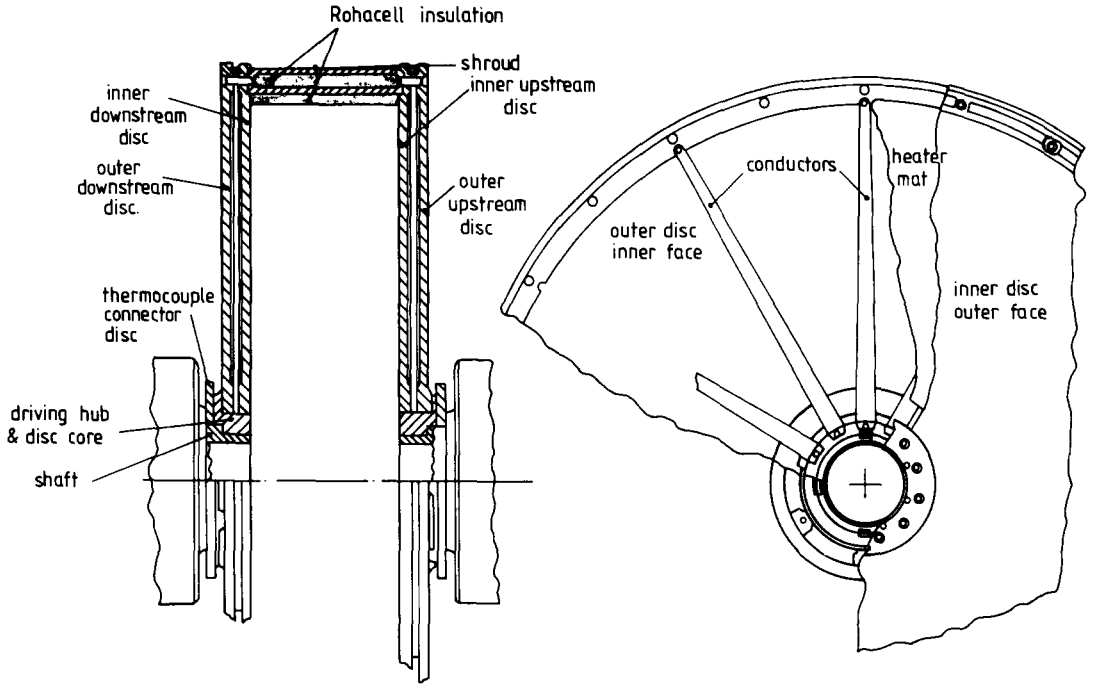


*Figure 2* Details of cavity assembly

was the same as that described above, the radius ratio was $a/b=0.100$, and a gap ratio of $G=0.133$ was tested.

### The air supply

The central hole in one of the discs (which is referred to below as the downstream disc) was sealed with a thin layer of epoxy-resin-impregnated glass-fiber sheet (the same material used for the thermocouple mats described in I). Air entered the cavity axially through the center of the other disc (the upstream disc) and left through the holes in the shroud.

The air was supplied by a centrifugal blower, after which it passed through a diffuser, heat exchanger, and contraction. From the contraction, it entered the cavity via the upstream hollow rotating shaft; the junction between the stationary contraction and the rotating shaft was sealed to minimize leakage. For low flow rates ($C_w<7000$), a 250 W Secomak blower was used, and the flow rate was measured by means of Annubar differential pressure devices. For high flow rates, ($C_w>7000$), an 18 kW Alldays and Peacock blower was used, and the flow rate was measured by a venturi nozzle. The accuracy of the flow measurement was estimated to be 3%, and details of the calibrations are given in Ref. 12.

The heat exchanger was used to reduce the temperature of the cooling air to that of the surrounding atmosphere ($\sim 20°C$), and the temperature of the air entering the cavity was measured by a thermocouple probe fitted in the contraction immediately upstream of the rotating shaft. The signals from this thermocouple and from the thermocouples and fluxmeters on the composite discs were measured by the data logger described in I.

### Optical instrumentation

For the flow visualization tests, the upstream disc and shroud were made from transparent polycarbonate, and the cavity was illuminated by a 4 W argon-ion laser used in conjunction with a cylindrical lens. This created "slit illumination" of either the $r$-$z$ plane (a plane through the axis of rotation) or the $r$-$\phi$ plane (normal to the axis). A Concept smoke generator was used to produce clouds of micron-sized oil particles which were injected, in short bursts, into the air entering the cavity. A sequence of photographs was taken from the time the smoke entered the cavity to the time it had been convected to all regions of interest.

Further details of the optical techniques, together with photographs of the flow structure in a rotating cavity, are included in Ref. 13.

### Data analysis

The heat transfer instrumentation was essentially the same as that described in I, and local Nusselt numbers were determined in two ways: using the solution of Laplace's conduction equation and using four of the five fluxmeters located in the front (cavity-side) face of each disc; fluxmeter number 4 failed on both discs.

The boundary conditions used for the solution of Laplace's equation (referred to below as the "conduction solution") were the same as those used in I, except for the outer radius. It was considered appropriate to model the outer surface of each disc and the shroud as a rotating cylinder which convected heat into the surrounding air, and the relationship given by Kays and Bjorklund[14] was used to determine the heat transfer coefficient. The outer shroud was treated as an annular fin that convected heat to both the surrounding air and to the cooling air flowing through the central holes. An effective conductance of 175 W/m$^2$ K for the interface between the shroud and the disc was found to produce the "best" results for the tests, conducted by Long,[15] that were used to validate the numerical solutions. Also included in that reference are details of a model to account for radiation from the disc surfaces. In the tests reported below, both discs were at essentially the same temperature, and the radiation corrections were negligible.

In I, the fluxmeters were calibrated in situ using the conduction solution for the free disc to determine the fluxes. For the results presented below, the fluxmeters were recalibrated in situ by Long,[16] using an impinging jet of air on the front face of the disc while the back face and periphery were insulated with

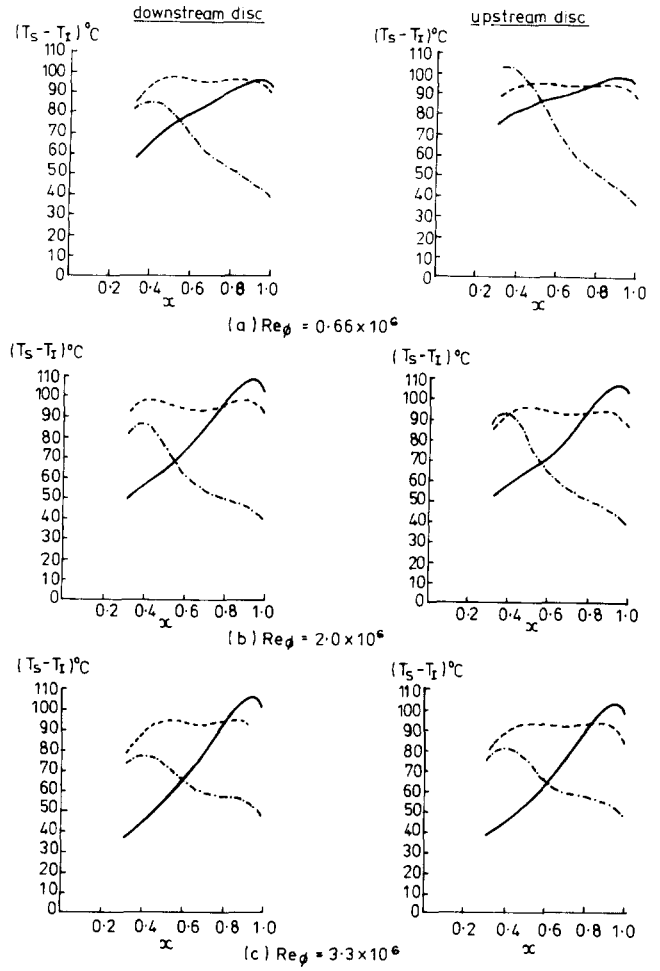


*Figure 3* Typical radial temperature profiles for $C_w = 7000$: ——, positive profile; – – –, constant profile; — · —, negative profile

Rohacell foam to minimize heat losses. The calibration was based on a simple theoretical model which treated the fluxmeter as a thermopile embedded in a thin film of Kapton insulation. Three calibration constants were determined by statistical regression of the measured and predicted fluxes, and these constants were consistent with those calculated from the physical properties of the fluxmeter materials. For the range of fluxes used in I, differences between the two different calibrations were small.

## Experimental measurements

### The disc surface temperatures

The radial distribution of temperature on the front (cavity-side) faces of the discs could be altered by varying the power input to the five annular heaters in each disc. For the heat transfer tests discussed below, the discs were "symmetrically heated": the radial distribution of power was the same for each disc. However, since the cooling air could impinge on the downstream disc, the resulting temperature distributions were not exactly symmetrical. Also, despite the thermal insulation between the heaters and the back faces of the discs, not all the input power passed through the front faces.

Three different temperature profiles were used to determine the effect of the surface temperature on heat transfer inside the cavity. For these profiles, attempts were made to produce temperatures that increased, decreased, or were constant with increasing radius (referred to below as positive, negative, and constant profiles, respectively), and examples are shown in Figure 3 for $C_w = 7000$. To avoid confusion, the data points are omitted, and only the smoothing curves, which were used as boundary conditions for the solutions of the conduction equation and of the integral equations, are shown. For most tests, the maximum surface temperature and the coolant inlet temperature were approximately 120°C and 20°C, respectively.

In Figure 3(a), for $Re_\phi = 0.66 \times 10^6$, it can be seen that there are differences between the temperature distributions for the two discs. This, as stated above, was caused by the cooling air impinging on the downstream disc, thereby reducing the temperature at the smaller radii. The asymmetry decreases with increasing Reynolds number, as can be seen in Figure 3(c) for $Re_\phi = 3.3 \times 10^6$. Despite any asymmetries, there are clear differences between the three radial temperature profiles.

### Flow visualization

For the flow visualization tests, the upstream disc and shroud were made from transparent polycarbonate, and either the $r$-$z$ or $r$-$\phi$ plane of the cavity was illuminated by the argon-ion laser. Pulses of smoke from the Concept generator were injected into the cooling air, and the resulting flow patterns were observed directly. Unfortunately, all the photographs that were taken were spoiled in processing, and the reader is referred to Pincombe[13] for photographic evidence and for further details of the optical technique.

The observed flow structure was broadly similar to that shown in Figure 1, and there was clear evidence of the source region, Ekman layers, sink layer, and inviscid core. The edge of the source region was determined by marking its location on the polycarbonate disc while it was rotating, and the dimensionless radius, $x_e$, was measured when the disc was stationary. The estimated accuracy of the measurements, which were made using both $r$-$z$ and $r$-$\phi$ illumination, was $\pm 10$ mm, which corresponds to an error of $\pm 0.02$ in the measured value of $x_e$.

Figure 4 shows the measured variation of $x_e$ with $Re_\phi$ for isothermal flow with $C_w = 950$, 1400, 2800, and 6610. Also shown are the curves corresponding to Equations 1 with

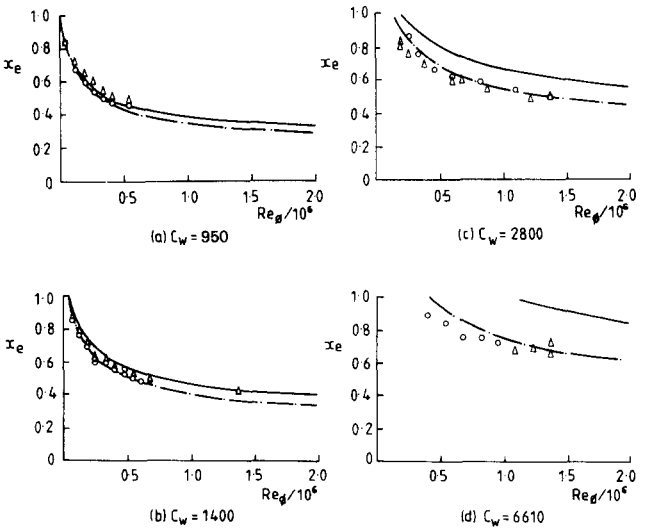


*Figure 4* The effect of $C_w$ on the variation of $x_e$ with $Re_\phi$: ○, measurements with $r$-$z$ illumination; △, measurements with $r$-$\phi$ illumination; ——, Equation 1 with $A = 0.599$; — · —, Equation 1 with $B = 1.79$

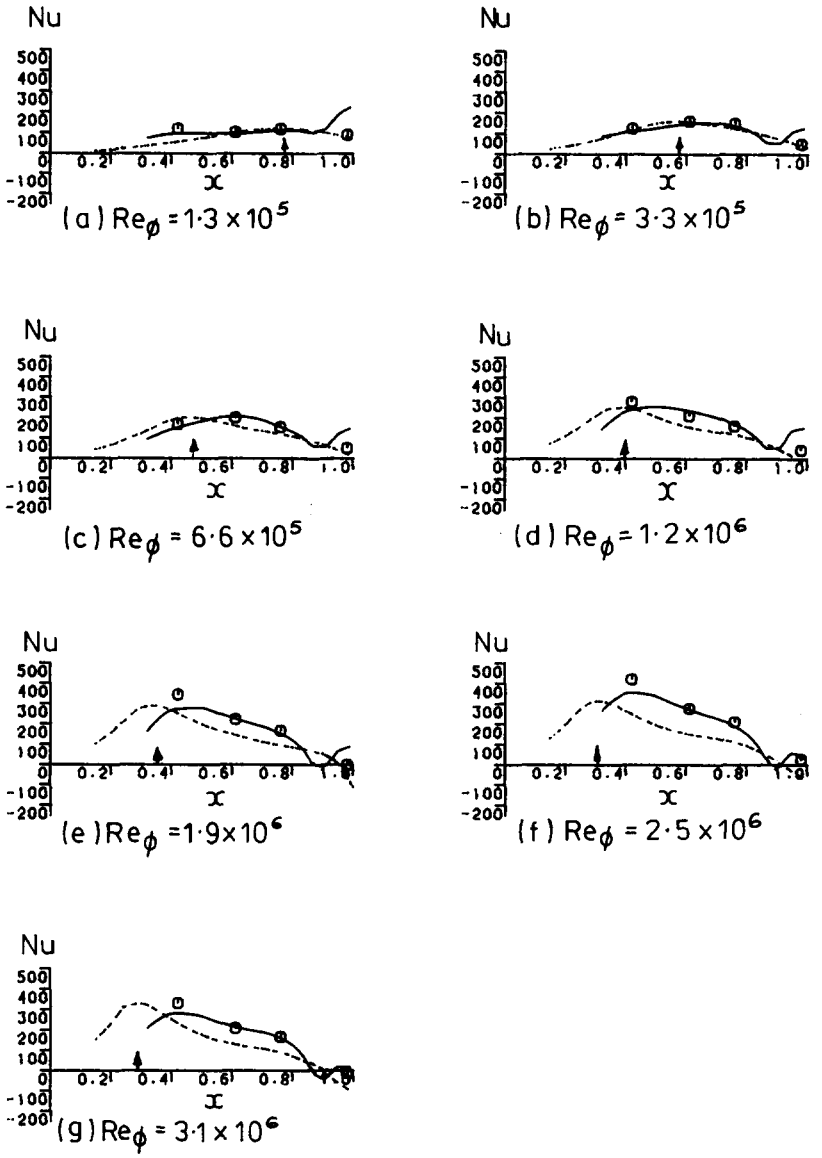


*Figure 5* The effect of $Re_\phi$ on the variation of Nu with $x$ for a positive temperature profile: $C_w = 1400$; downstream disc: O, fluxmeter measurement; ———, conduction solution of Long [15]; – – –, theory of Chew and Rogers[11]; ↑, edge of source region

$A = 0.599$ and $B = 1.79$ for laminar and turbulent flow, respectively. Using $Re_r = 180$ as the criterion for transition from laminar to turbulent flow in the Ekman layers, the flow should be turbulent throughout the cavity for $C_w \geq 1130$; for $C_w = 950$, the flow should be turbulent for $x \leq 0.8$. The agreement between the measured data and the theoretical curves is generally good: a regression analysis using over 60 data points from $x_e = 0.42$ to 0.90 gave the constant of proportionality in Equation 1 as 1.80 compared with the theoretical value of 1.79.

A number of tests were made with the downstream disc heated to produce a positive temperature profile and a maximum temperature of 50°C. The measured values of $x_e$ were slightly larger than those obtained for isothermal flow, but since there were only seven results, for $C_w = 1400$ and $1.4 < Re_\phi / 10^5 < 6.8$, no firm conclusions could be drawn. However, for nonisothermal tests in the range $490 < C_w < 1400$ and $Re_\phi < 7 \times 10^5$, it was observed that there were nonaxisymmetric oscillations in the source region for $Re_\phi \gtrsim 420 C_w$. These oscillations, which were not present for isothermal flow, were consistent with those seen under similar conditions on another rig by Owen and Onur.[4]

## Local Nusselt numbers

Figures 5 to 9 show the radial variation of local Nusselt number for various values of $C_w$ and $Re_\phi$. The experimental data correspond to the fluxmeter measurements and to the conduction solution of Long[15] described in the third section. The theoretical curves were obtained from a program based on the method of Chew and Rogers[11] referred to in the second section. Also shown, where appropriate, is the radial location of the edge of the source region according to Equation 1 with $B = 1.79$ for turbulent flow.

Figure 5 shows the Nusselt numbers, for the downstream disc with a positive temperature profile, for $C_w = 1400$ and $1.3 \times 10^5 < Re_\phi < 3.1 \times 10^6$. For this and higher values of $C_w$, the flow in the Ekman layers is expected to be turbulent: that is, $Re_r > 180$ for all values of $x$. The agreement between the

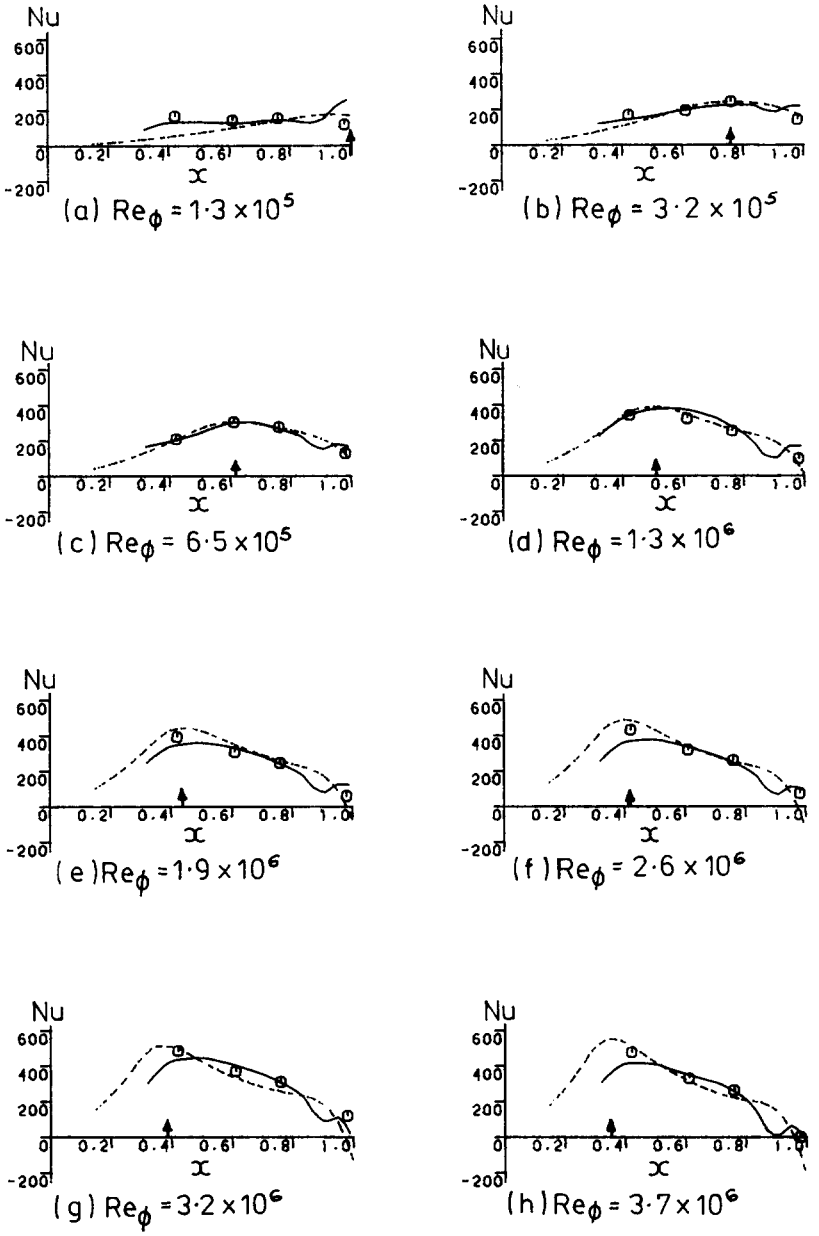


*Figure 6* The effect of $Re_\phi$ on the variation of Nu with $x$ for a positive temperature profile: $C_w = 2800$; downstream disc: ○, fluxmeter measurement; ———, conduction solution of Long[15]; – – –, theory of Chew and Rogers[11]; ↑, edge of source region

conduction solution and the fluxmeter measurements is generally good except, for the lower values of $Re_\phi$, near the outer edge of the disc where the conduction solution is expected to be less accurate. The agreement between theory and experiment is good at the lower values of $Re_\phi$, but at the higher values the theoretical curve underpredicts the measured Nusselt numbers. However, for this value of $C_w$ the heat fluxes are relatively small, and experimental errors tend to be larger than for the higher values of $C_w$.

The results obtained for the upstream disc were almost identical to those shown in Figure 5 for the downstream disc. It can be seen that Nu reaches a maximum at a radial location corresponding, approximately, to the edge of the source region, and the maximum value increases with increasing $Re_\phi$. The increase of Nu with $x$ in the source region is associated with an entraining boundary layer, which has characteristics similar to those of the free disc. In the Ekman layers, no entrainment occurs, and in the outer part of the cavity the temperature of the fluid approaches that of the disc. Consequently, the heat flux in the Ekman layers decreases with increasing $x$, resulting in a reduction of Nu, as predicted by Equation 2.

Figure 6 shows the radial distribution of Nu for the downstream disc with a positive temperature profile for $C_w = 2800$; the results obtained for the upstream disc were very similar. The magnitudes of the Nusselt numbers are generally higher than those shown in Figure 5, and the agreement between the theoretical curves and the fluxmeter measurements for $C_w = 2800$ is much better than for $C_w = 1400$. In all other respects, the comments made about the results presented in Figure 5 are applicable to Figure 6.

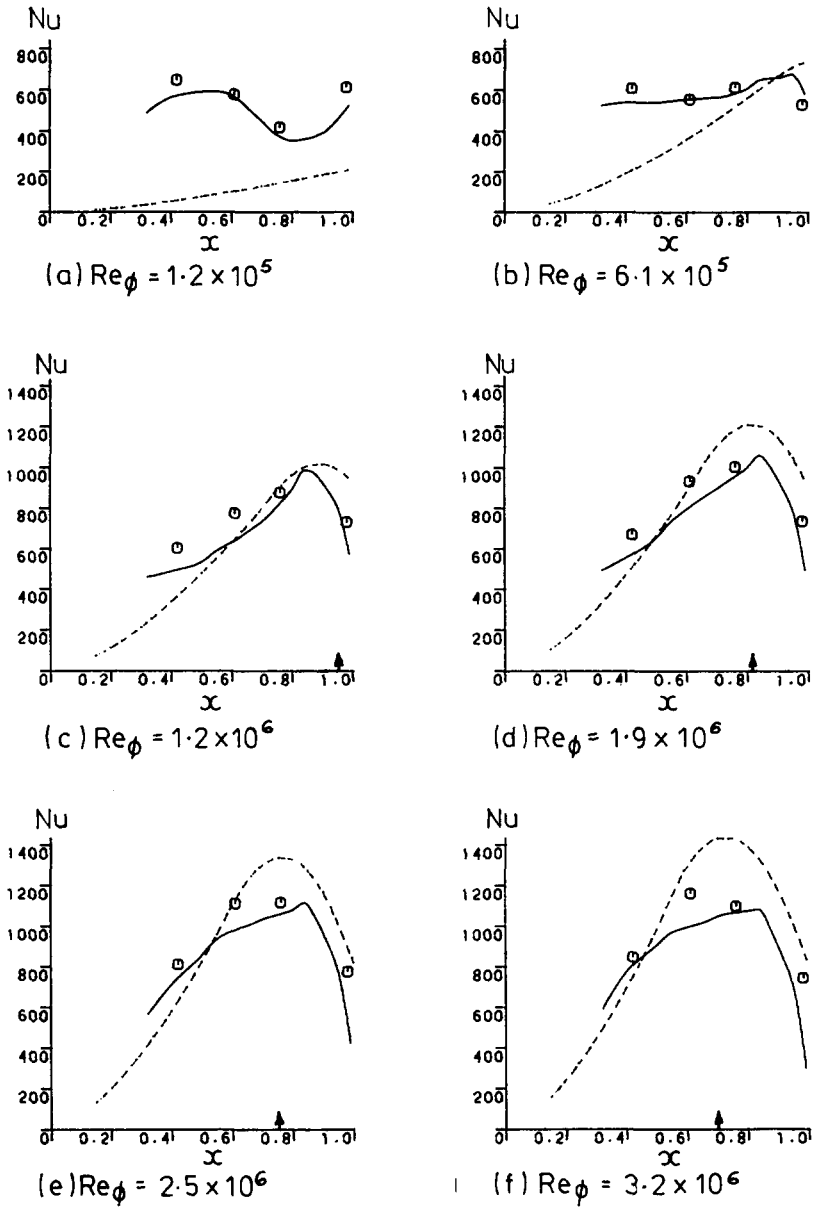


*Figure 7* The effect of $Re_\phi$ on the variation of Nu with $x$ for a positive temperature profile: $C_w = 14{,}000$; downstream disc: O, fluxmeter measurement; ———, conduction solution of Long[15]; – – –, theory of Chew and Rogers[11]; ↑, edge of source region; — — —, Equation 5

Figures 7 and 8 show the results for the downstream and upstream discs, respectively, for $C_w = 14{,}000$ with positive temperature profiles on the discs. According to Equation 1, for turbulent flow with $B = 1.79$, the source region fills the entire cavity (that is, $x_e > 1$) when

$$Re_\phi < 6.6\, C_w^{5/4} \tag{4}$$

For $C_w = 14{,}000$, Equation 4 implies that Ekman layer flow cannot occur for $Re_\phi < 10^6$. Under these conditions, the wall-jet correlation of Long[17], where

$$Nu = 1.46\, G^{1/6} C_w^{2/3} \tag{5}$$

is applicable for the downstream disc. For $C_w = 14{,}000$ and $G = 0.138$, Equation 5 gives $Nu = 610$, which provides a reasonable approximation to the measured values in Figures 7(a) and (b). For $Re_\phi \geqslant 1.2 \times 10^6$, where Ekman layer flow is expected to occur over part of the disc surface, the agreement between the theoretical curves and the experimental data in Figures 7 and 8 is significantly better than for the small values of $Re_\phi$.

The above Nusselt numbers were all obtained for discs with positive temperature profiles, whereas Figure 9 shows results for the positive, constant, and negative temperature profiles described in the subsection on the disc surface temperatures. The measurements were made on the upstream disc for $C_w = 7000$; the outermost fluxmeter was not working on the downstream disc, but in all other respects the two sets of results were very similar.

For $C_w = 7000$, Ekman layer flow is expected to occur over a significant part of the disc for all the Reynolds numbers tested. Figure 9 shows that, in the main, agreement between the fluxmeters, conduction solution, and theory is good. The

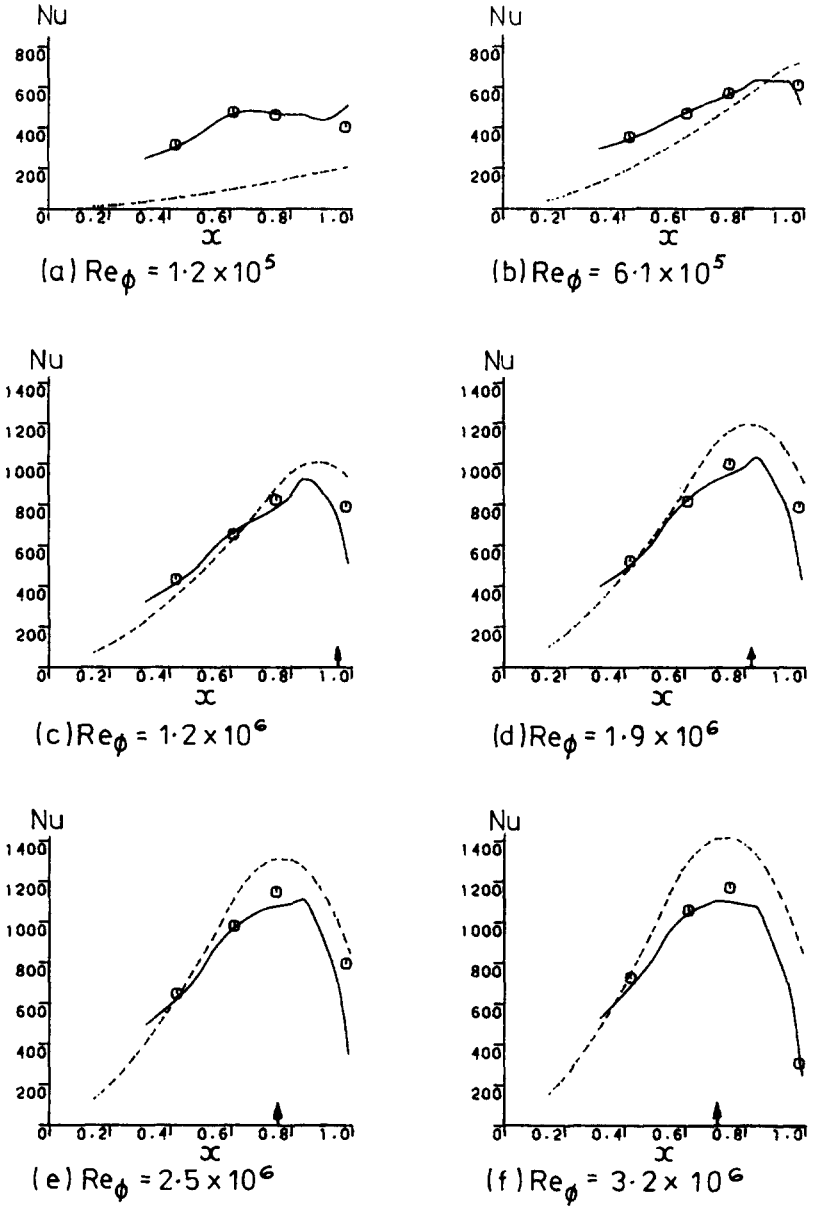


*Figure 8* The effect of $Re_\phi$ on the variation of Nu with $x$ for a positive temperature profile: $C_w$=14,000; upstream disc: O, fluxmeter measurement; ———, conduction solution of Long[15]; – – –, theory of Chew and Rogers[11]; ↑, edge of source region

maximum value of Nu coincides approximately with the edge of the source region, and the Nusselt numbers increase with increasing $Re_\phi$. The effect of temperature profile is significant, particularly in the Ekman layers where the values of Nu for the negative profile (Figures 9(c), (f), (i)) are smaller than those for the positive profile (Figures 9(a), (d), (g)); the results for the constant temperature (Figures 9(b), (e), (h)) are intermediate.

An interesting result is that in Figures 9(f), (h), and (i), negative Nusselt numbers occur at the outer radii. This effect, which is confirmed theoretically and experimentally, occurs when the temperature of the fluid in the nonentraining Ekman layers exceeds that of the disc: heat transferred from the disc to the fluid at the smaller radii is transferred back to the disc at the larger radii. From the definition of Nu given in Equation 3, if $q < 0$ and $(T_S - T_I) > 0$ then the Nusselt number will be negative.

In conclusion, the agreement between the theoretical and experimental Nusselt numbers for this range of conditions gives confidence in both techniques.

## Conclusions

Flow visualization and heat transfer measurements have been made in a rotating cavity with a radial outflow of cooling air for rotational Reynolds numbers up to $Re_\phi = 3.3 \times 10^6$ and dimensionless flow rates up to $C_w$=14,000. Flow visualization has confirmed that the flow structure comprises a source region, Ekman layers, a sink layer, and an interior core of rotating fluid, and the measured size of the source region is in good agreement with the value predicted from a simple theoretical model.

Local Nusselt numbers have been determined experimentally from fluxmeters and from the numerical solution of Laplace's

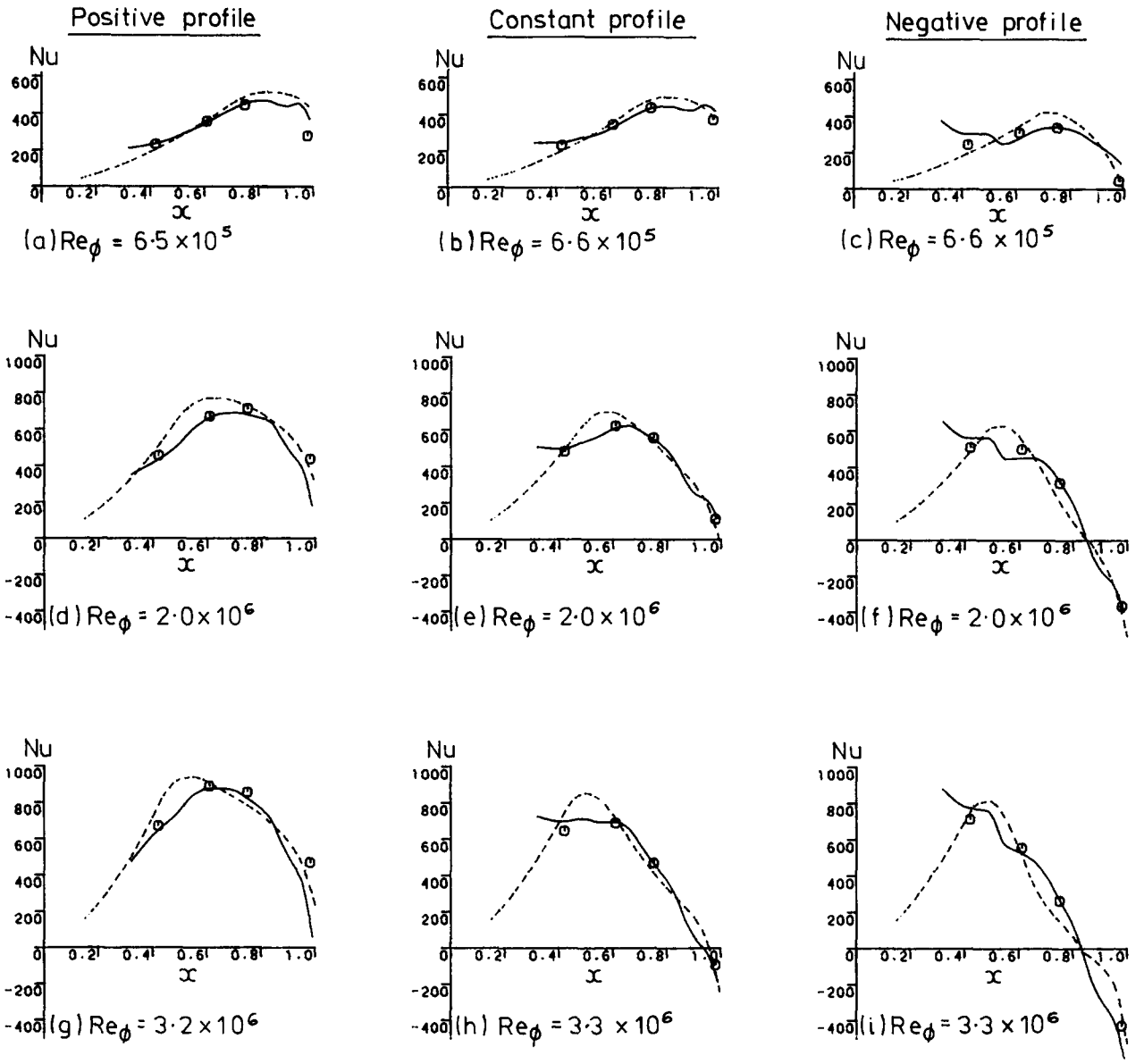


*Figure 9* The effect of temperature profiles and $Re_\phi$ on the variation of Nu with $x$: $C_w = 7000$; upstream disc: O, fluxmeter measurement; ———, conduction solution of Long[15]; – – –, theory of Chew and Rogers[11]

conduction equation, and these results have been compared with theoretical curves obtained from numerical solutions of the integral turbulent momentum and energy equations using the method of Chew and Rogers.[11] Results were obtained for the upstream and downstream discs of a symmetrically heated cavity: the radial distribution of the internally generated heat flux was the same for each disc.

Provided that the source region did not fill the entire cavity, the agreement between theory and experiment was generally good. A maximum value of Nusselt number occurred near the edge of the source region, and Nu increased with increasing $C_w$ and $Re_\phi$. It was also shown that the Nusselt numbers were strongly influenced by the radial distribution of surface temperature, particularly for the outer part of the disc covered by the Ekman layers. The Nusselt numbers tended to be smaller for a "negative profile" (where the temperature decreased with increasing radius) than for a "positive profile," and, under some conditions, negative Nusselt numbers at the outer radii were predicted theoretically and measured experimentally.

If the flow rate is large enough for the source region to fill the entire cavity, a wall jet forms on the downstream disc, resulting in higher rates of heat transfer at the smaller radii. Under these conditions, the theoretical model, which takes no account of wall-jet flow in the source region, underestimates the Nusselt numbers. However, for air-cooled gas turbine discs, for which application the research is intended, the flow rates are unlikely to be high enough to create the "wall-jet" effect, and the theoretical model should provide a very useful design tool.

## Acknowledgments

The authors are indebted to SERC, Rolls-Royce plc, and Ruston Gas Turbines plc for funding the research described in this two-part paper. We also wish to thank Dr. Long and Dr. Rogers for the computation of the conduction solutions and theoretical curves, respectively, presented in Part 2. Last, but not least, we acknowledge the skill and forbearance of the

technicians who not only built the rig but assisted in getting it to produce results!

## References


1 Northrop, A. and Owen, J. M. Heat transfer measurements in rotating-disc systems. Part 1: The free disc. *Int. J. Heat Fluid Flow*, 1988, **9**, 19–26

2 Hide, R. On source-sink flows in a rotating fluid. *J. Fluid Mech.*, 1968, **32**, 737

3 Owen, J. M. and Pincombe, J. R. Velocity measurements inside a rotating cylindrical cavity with a radial outflow of fluid. *J. Fluid Mech.*, 1980, **99**, 111

4 Owen, J. M. and Onur, H. S. Convective heat transfer in a rotating cylindrical cavity. *J. Engng. Power*, 1983, **105**, 265

5 Chew, J. W., Owen, J. M., and Pincombe, J. R. Numerical predictions for laminar source-sink flow in a rotating cylindrical cavity. *J. Fluid Mech.*, 1984, **143**, 451

6 Owen, J. M., Pincombe, J. R., and Rogers, R. H. Source-sink flow inside a rotating cylindrical cavity. *J. Fluid Mech.*, 1985, **155**, 233

7 Firouzian, M., Owen, J. M., Pincombe, J. R., and Rogers, R. H. Fluid dynamics and heat transfer in a rotating cylindrical cavity with a radial inflow of fluid. Part 1: The flow structure. *Int. J. Heat Fluid Flow*, 1985, **6**, 228

8 Firouzian, M., Owen, J. M., Pincombe, J. R., and Rogers, R. H. Fluid dynamics and heat transfer in a rotating cylindrical cavity with a radial inflow of fluid. Part 2: Velocity, pressure and heat transfer measurements. *Int. J. Heat Fluid Flow*, 1986, **7**, 21

9 Long, C. A. and Owen, J. M. The effect of inlet conditions on heat transfer in a rotating cavity with a radial outflow of fluid. *J. Turbomachinery*, 1986, **108**, 145

10 Northrop, A. and Owen, J. M. Heat transfer measurements in the modified Mark II rotating cavity rig. Part 2: Rotating cavity tests. Report No. 83/TFMRC/59, School of Engineering and Applied Sciences, University of Sussex, 1983

11 Chew, J. W. and Rogers, R. H. An integral method for the calculation of turbulent forced convection in a rotating cavity with radial outflow. *Int. J. Heat Fluid Flow*, 1988, **9**, 37–48

12 Northrop, A. Heat transfer in a cylindrical rotating cavity. D. Phil. thesis, University of Sussex, 1984

13 Pincombe, J. R. Optical measurements of the flow inside a rotating cylinder. Ph.D. thesis, University of Sussex, 1983

14 Kays, W. M. and Bjorklund, I. S. Heat transfer from a rotating cylinder with and without crossflow. *Trans. ASME*, 1958, **80**, 170

15 Long, C. A. Transient analysis of experimental data from the Mark II rotating cavity rig. Report No. 85/TFMRC/76, School of Engineering and Applied Sciences, University of Sussex, 1985

16 Long, C. A. Calibration of the fluxmeters on the Mark II rotating cavity rig. Report No. 86/TFMRC/88, School of Engineering and Applied Sciences, University of Sussex, 1986

17 Long, C. A. Transient heat transfer in a rotating cavity. D. Phil. thesis, University of Sussex, 1984